ARTICLES

Liquid Crystal Properties of the *n*-Alkyl-cyanobiphenyl Series from Atomistic Simulations with *Ab Initio* Derived Force Fields

Ivo Cacelli,* Luca De Gaetani,† Giacomo Prampolini,‡ and Alessandro Tani§

Dipartimento di Chimica e Chimica Industriale Universita di Pisa, via Risorgimento 35, I-56126 Pisa, Italy

Received: September 6, 2006; In Final Form: November 30, 2006

Lengthy molecular dynamics (MD) simulations were performed at constant atmospheric pressure and different temperatures for the series of the 4-*n*-alkyl-4′-cyanobiphenyls (*n*CB) with $n = 6$, 7, and 8. The accurate atomistic force field (Bizzarri, M.; Cacelli, I.; Prampolini, G; Tani, A. *J. Phys. Chem. A* **2004**, *108*, 10336), successfully employed to reproduce thermodynamic and transport properties of the 5CB molecule, has here been extended to higher homologues. Nematic and isotropic phases were found for all members of the series, and also, a smectic phase was (tentatively) identified for 8CB at 1 atm and 300 K. Transition temperatures reproduce the experimental values within ±10 K. Also, structural properties as second and fourth rank orientational order parameters are in good agreement with the corresponding experimental quantities. This means that the well-known odd−even effect, observed for many properties along the *n*CB series, is well reproduced, despite the narrow range of oscillations, e.g., in clearing temperatures. A detailed analysis of the correlation between molecular properties and odd−even effects is presented.

1. Introduction

Liquid crystals (LC) certainly constitute a fascinating challenge in the study of structure−properties relationships, as they show an extreme sensitivity to small changes in chemical background. In some banana shaped molecules,[1] for instance, the substitution of an aromatic core hydrogen atom with a chlorine causes[2] the disappearance of a highly ordered B_2 phase in favor of a nematic one. The *p*-terphenyl molecule has been found[3] to yield a variety of liquid crystalline phases, depending on the fluorination site. Another example can be found in the 4-cyano-4′-*n*-alkylbiphenyl series (*n*CB), where the addition of a methylene group in the alkyl chain may induce stable nematic (5CB−8CB) and smectic (8CB) mesophases.[4−6] This extraordinary sensitivity to the details of molecular structure arises[7,8] from a complex interplay between energetic effects (the molecular interactions through electrostatic, dispersive, and inductive forces) and entropic ones (positional, orientational, and conformational distributions). From a thermodynamic point of view, the balance among these terms introduces those small free energy differences that can affect the (meso)phase relative stability. Small variations in the molecular framework can alter this delicate equilibrium, causing evident changes not only in the phase diagram[4,9−11] but also in industrially important properties,[12] e.g., dielectric permittivity[13,14] or the rotational viscosity coefficient.[15] In particular, aliphatic flexible chains can perturb the energetic−entropic balance in a very complex manner, giving rise to phenomena such as the well-known odd−even effect in nematics or the appearance of the smectic phase for larger homologues.[4,7,9−11] In conclusion, the characteristics of liquid crystalline materials are intrinsically strongly linked to both single molecule (electronic structure or flexibility) and collective properties (long range ordering or viscosities), and a full comprehension of this relationship requires a detailed understanding of the microscopical background.

In such investigations, molecular dynamics (MD) techniques appear as a natural choice[16−19] as they link a molecular description entailed in the adopted force field (FF) with the resulting macroscopic bulk properties. Even if long dynamics are needed in order to recover reliable information on the structure of LC phases, full atomic (FA) FFs can still be adopted[17−23] thanks to the continuous increase of the computational resources. Unfortunately, the most employed literature FFs[24−27] are effective potentials, designed to reproduce a few macroscopic features of a chosen group of molecules in a determined thermodynamic range, but none were parametrized to reproduce LC properties. The lack of accurate FFs, together with the high demand of computational resources, has lead some authors to judge the reproduction of LC transition temperatures to be impossible[28] or to question the ergodicity of simulated LC systems.[29] Recent works[18−20,22] have shown that the reproduction of some LC properties can be achieved through some corrections to the literature FF, as, for example, the reparametrization of the point charges through the fitting of quantum mechanical results. In particular, following this method, Berardi et al.[22] have reproduced the odd−even effect on the transition temperatures of the phenyl alkyl-4-(4′-cyanobenzylidene) amminocinnamate series, performing simulations of more than 30 ns on systems of 98 molecules. On the contrary, the straightforward adoption of literature parameters has led to over-[30] or underestimations[31] of the orientational ordering of

* E-mail: ivo@dcci.unipi.it.
† E-mail: degaetani@dcci.unipi.it.
‡ E-mail: giacomo@dcci.unipi.it.
§ E-mail: tani@dcci.unipi.it.

10.1021/jp065806l CCC: $37.00
Published on Web 02/09/2007

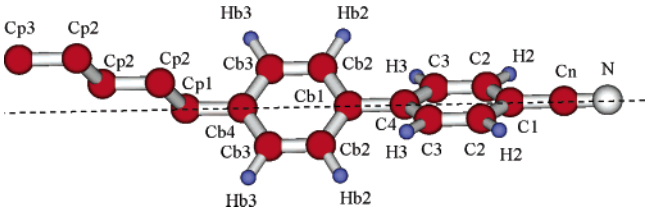

Figure 1. Model for the 5CB molecule. Extension to higher homologues has been obtained by adding a number of Cp2 sites to the aliphatic chain. The dashed line indicates the *n*CB core main axis.

similar nematogenic molecules, even if the short MD equilibration times (≃1 ns) and the dimensions of the explored systems (125 and 64 molecules for refs 30 and 31, respectively) pose some questions on the stability of the obtained phases.

Another route to obtain FFs suitable for LC is to construct the model potential functions specifically for the molecule under study, deriving the FF parameters from *ab initio* information only. This alternative approach[32,33] has two major advantages: the molecular details can be entailed in the adopted FF up to the chosen level of accuracy, and the resulting properties do not rely on any experimental information. In principle, the latter feature gives the whole approach predictive capabilities. Following this route, a flexible FA model was recently proposed by our group for the 5CB molecule, where both the inter- and intramolecular parts were obtained through the use of the fragmentation reconstruction method (FRM)[34,35] and accurate density functional theory (DFT) calculations,[23] respectively. MD simulations, performed with this FF, have proven capable of reproducing with good accuracy both the thermodynamic[23] and the transport properties[36] of the 5CB molecule.

A further and more severe test of the accuracy of this first principles approach can be carried out extending the aforementioned 5CB FF to the higher *n*CB homologues ($n = 6-8$). Indeed, the *n*CBs have been widely studied[5,6,9,37−42] so that experimental results of several quantities are available for comparison. Moreover, the series presents both a variety of mesophases and typical odd−even effects in a number of properties, e.g., clearing temperatures. In the *n*CB case, the odd−even effect occurs in a fairly narrow range of temperatures (≃10 K), so that its reproduction represents a challenge for the whole modeling approach. As a consequence, a successful outcome would constitute a further, encouraging step toward predictivity.

This paper is organized as follows. In Section 2, we discuss the model potentials employed, the main computational details of MD simulations, and some of the monitored observables. In Section 3, the MD results are collected, and the computed properties are compared with the experiment and discussed.

2. Computational Details

2.1. Model Potentials. The FF adopted for 5CB[23,35] is a FA representation with the exception of the aliphatic hydrogens, which were considered together with each aliphatic carbon as single interaction sites, as shown in Figure 1.

The potential energy, adopted in the 5CB simulations,[23,36] has the following AMBER-like[43] expression:

$$E_{tot} = E_{LJ} + E_{Coul} + E_{stretch} + E_{bend} + E_{tors} + E_{LJintra} \quad (1)$$

where the intramolecular terms are given by the standard forms,

$$E_{stretch} = \sum_{i}^{N_{bonds}} k_i^s (r_i - r_i^0)^2 \qquad E_{bend} = \sum_{i}^{N_{angles}} k_i^b (\theta_i - \theta_i^0)^2 \quad (2)$$

$$E_{tors} = \sum_{i}^{N_{dihedrals}} \sum_{j}^{N_{cos_i}} k_{ij}^d [1 + \cos(n_j^i \delta_i - \gamma_j^i)]$$

$$E_{LJintra} = \sum_{i}^{N_{LJintra}} \sum_{j=i+4,i+5,\ldots} u_{ij}^{LJ} \quad (3)$$

u_{ij}^{LJ} has the form of the standard 12−6 Lennard-Jones potential. With regard to the intermolecular interaction, the long-range electrostatic potential has been computed as

$$E_{Coul} = \sum_{i=1}^{N_{sites}} \sum_{j \geq i}^{N_{sites}} \frac{q_i q_j}{r_{ij}} \quad (4)$$

where i and j belong to different molecules and N_{sites} is the total number of interacting sites. Finally, for the short-range part, a suitably modified[35] Lennard-Jones term has been employed:

$$E_{LJ} = \sum_{i=1}^{N_{sites}} \sum_{j \geq i}^{N_{sites}} u_{ij}^{LJmod} \quad (5)$$

with

$$u_{ij}^{LJmod} = 4\epsilon_{ij}\left[\left(\frac{\xi_{ij}\sigma_{ij}}{r_{ij} + \sigma_{ij}(\xi_{ij} - 1)}\right)^{12} - \left(\frac{\xi_{ij}\sigma_{ij}}{r_{ij} + \sigma_{ij}(\xi_{ij} - 1)}\right)^{6}\right] \quad (6)$$

The inter- and intramolecular parameters as well as their derivation are reported in detail in refs 35 and 23, respectively.

The model has been here transferred to the higher homologues through the addition of one, two, or three Cp2 interaction sites for 6CB, 7CB, and 8CB, respectively. The extension of the intermolecular part of the FF can be easily achieved because all Cp2 sites of 5CB were considered as equivalent, thus possessing the same intermolecular parameters. Moreover, because each Cp2 was considered chargeless, the addition of a Cp2 site does not alter the electroneutrality of the molecule. Concerning the intramolecular part, the bending and torsional parameters used to describe the flexibility of the 5CB aliphatic chain can be now used to mimic the new degrees of freedom resulting from the chain elongation. To prevent a nonphysical curling of the chain on the aromatic core, LJ intramolecular interactions were added[23] in the 5CB molecule between the last three sites of the pentyl moiety and the aromatic CB*n* ($n = 1-4$) carbons. Such interactions have been kept for all *n*CB homologues. Furthermore, to prevent the curling of the flexible chain over itself in 7CB and 8CB, intramolecular LJ interactions were extended to Cp2−Cp2 and Cp3−Cp2 pairs more than four bonds apart.

2.2. Simulations. All MD simulations were carried out in the NPT ensemble with a parallel version of a modified[23] Moscito3.9[44] package. Temperature and pressure were kept constant using the weak coupling scheme of Berendsen et al.,[45] allowing the aspect ratio of the simulation cell to vary during simulation runs. Starting configurations were prepared following the same procedure for all *n*CBs. First, a complete optimization of each molecular geometry was performed through quantum mechanical calculations, carried out with the density functional B3LYP method[46] using a polarized triple ζ 6-311G(2d,p) basis set. After removing the aliphatic hydrogen atoms from each

optimized conformation, an antiparallel dimer arrangement was created. The *n*CB dimers were replicated 3 and 4 times along the *x* and *y* laboratory axis, respectively, to obtain a layer of 48 molecules. Finally, a low density, orientationally ordered ($\langle P_1 \rangle = 0$; $\langle P_2 \rangle = 1$) lattice was constructed by replicating each layer four times along the *z* axis. This way, we obtained 192 *n*CB molecules for a total of more than 5000 interaction sites. These low-density crystals were used as starting configurations for short, high pressure ($P = 1000$ atm) runs performed at $T = 100$ K. The final configurations were all characterized by high densities (>1.1 g/cm^3), high order parameters ($\langle P_2 \rangle > 0.65$), and some degree of positional order along the phase director. These systems were then equilibrated at atmospheric pressure and different temperatures. During all equilibration and production runs, the bond lengths were kept fixed at their equilibrium value using the SHAKE algorithm[47] and a time step of 1 fs was used. The short range intermolecular interactions have been truncated at $R_c = 10$ Å, employing standard corrections for energy and virial.[48] Charge−charge long range interactions were treated with the particle mesh Ewald (PME) method[49,50] using a convergence parameter α of $5.36/2R_c$ and a fourth-order spline interpolation.

The orientational order was studied calculating the major order parameter P_2, the mean fourth-rank Legendre polynomial P_4, and the orientational correlation functions $G_1(r)$ and $G_2(r)$.[51] P_2 was obtained by diagonalizing the Saupe ordering matrix $\mathbf{Q}$[52] defined as

$$Q_{ab} = \left\langle \frac{1}{2}(3u_a u_b - \delta_{ab}) \right\rangle \tag{7}$$

where the mean value $\langle ... \rangle$ is obtained averaging on all molecules composing the system and $\mathbf{u}$ ($a = x, y, z$) is the eigenvector corresponding to the minimum eigenvalue of the molecular inertia tensor, i.e., the principal axis. The maximum eigenvalue of $\mathbf{Q}$ is then taken as the principal order parameter P_2, and the corresponding eigenvector represents the phase director $\mathbf{n}$. The values of P_4 are obtained by averaging on all molecules the fourth Legendre polynomial

$$P_4 = \left\langle \frac{1}{8}(35\cos^4(\theta) - 30\cos^2(\theta) + 3) \right\rangle \tag{8}$$

where θ is the angle between the principal molecular axis $\mathbf{u}$ and the director $\mathbf{n}$. The orientational correlation functions $G_n(r)$ are obtained averaging, on all pairs of molecules and on time, the *n*-rank Legendre polynomial of the angle between the principal axis of two molecules as a function of their distance, i.e.,

$$G_n(r) = \langle P_n(\hat{u}_i \cdot \hat{u}_j) \rangle (r) \tag{9}$$

It is worth mentioning, as shown by Bates et al.,[53] that $G_2(r)$ reaches the asymptotic value of $\langle P_2 \rangle^2$ at large r.

The internal conformation of all homologues at different temperatures has been monitored, with particular attention to the torsional dihedrals and the elongation (L) of the aliphatic chain. The latter has been evaluated as the distance between the Cb4 site (Figure 1) and the projection of the Cp3 site on the long molecular axis. The distance of the Cp3 site from the long axis is then named $L_\perp$, and the ratio $L/L_\perp$ is labeled R_L. Their mean values, averaged on all molecules, will be indicated as $\langle L \rangle$, $\langle L_\perp \rangle$, and $\langle R_L \rangle$, respectively.

Another useful tool to describe the molecular "shape" is the aspect ratio of the moments of inertia, which is connected to the molecular aspect ratio:

$$\kappa_{mol} = \frac{(I_1 I_2)^{(1/2)}}{I_3} \tag{10}$$

Here, I_1 and I_2 are the two maximum eigenvalues of the molecular inertia tensor and I_3 is the minimum eigenvalue associated to the major axis of the molecules that are assumed to be rodlike. Finally, the inertia tensor anisotropy (ΔI) was computed as suggested by ref 22, that is,

$$\Delta I = \frac{(I_1 + I_2)/2 - I_3}{I_1 + I_2 + I_3} \tag{11}$$

3. Results and Discussion

3.1. Equilibration. Several NPT MD runs were performed for each *n*CB homologue, at $P = 1$ atm and temperature increasing from 290 to 330 K, with a step of 10 K. The equilibration of these runs was monitored observing potential energy, density, and order parameter. Whereas the first two observables equilibrate rather quickly (<1 ns), P_2 requires much longer times (>20 ns) to reach a steady state, as shown in Figure 2.

By looking for instance at the 6CB run at 310 K, it is clear that even 10 ns are not enough to assign a reliable equilibrium average value to P_2: to assess equilibrium, we have continued the simulation until the P_2 value did not drift for at least 15 ns. Although this approach rests more on conventional wisdom than on rigorous arguments, it represents a sensible balance between computational costs and requisite run lengths, such that it has also been adopted by other groups.[22]

It is evident from Figure 2 that all *n*CBs show both an orientationally ordered and a disordered phase. The analysis of the ordered phases shows the complete loss of the initial positional order, with the *n*CB molecular centers of mass exhibiting a liquid-like structure. This feature and the significant orientational order allow us to consider the latter phases as nematic. Moreover, because typical nematic phases show[7,10,11] an order parameter between 0.4 and 0.6, all systems whose P_2 dropped below 0.4 will be considered as isotropic liquids. Because the temperature scan was performed with a 10 K step, the clearing temperature (T_c) for the transition between the nematic and the isotropic phase can be assigned with an error of ±5 K. An exception is 6CB at 300 K, whose order parameter oscillates around 0.4 for more than 20 ns: T_c was located between 290 and 310 K, with a larger uncertainty (±10 K).

In the case of 8CB, in addition to a high order parameter ($\langle P_2 \rangle > 0.6$), we observed some positional order along the phase director at 300 K, i.e., in the experimental[5,6] range of existence of the smectic phase (294.5 and 306.5 K). Investigations on the 8CB smectic phase stability, as well as on the size effect on such systems, are currently in progress in our group[54] through computer simulations with a larger number of molecules.

3.2. Thermodynamic and Structural Properties. Once equilibration was assessed, thermodynamic properties of the nematic phases were averaged over 5 ns. Conversely, with regard to the isotropic phases, we adopted the following time-saving procedure to remove the residual orientational order ($\langle P_2 \rangle \simeq 0.3$). First, each system with $\langle P_2 \rangle$ below 0.4 and with a decreasing trend was heated at 400 K, until complete isotropization of the sample ($\langle P_2 \rangle < 0.2$). The system was then cooled back to the original temperature and further equilibrated for 3 ns. The resulting disordered phases were then employed as starting configurations for the production runs and to calculate the average properties in the isotropic liquid phase.

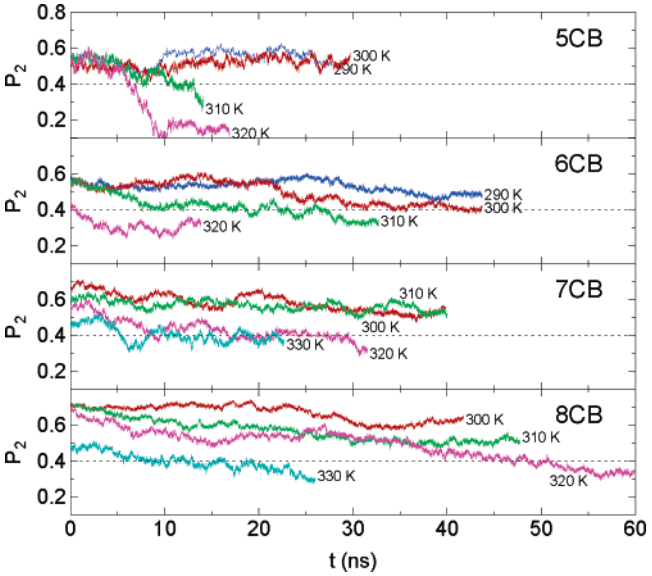

Figure 2. Equilibration runs at atmospheric pressure. The order parameter P_2 is monitored as a function of the simulation time at different temperatures for all the members of the *n*CB series; 5CB results are from ref 23. The dotted lines at $P_2 = 0.4$ mark the assumed lower bound of the nematic phase.

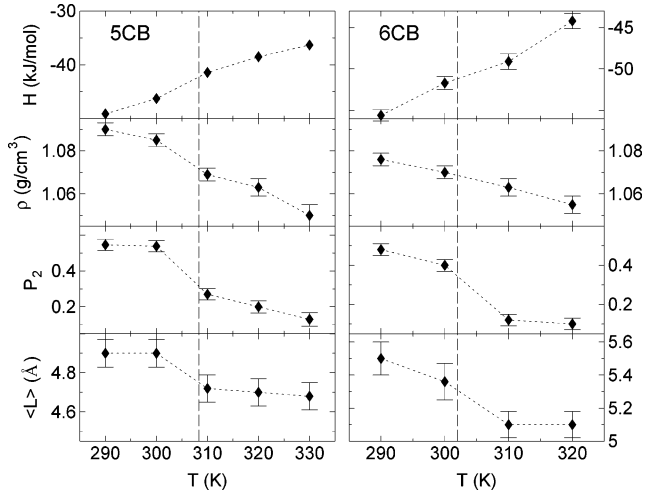

Figure 3. Thermodynamic properties as a function of temperature for 5CB and 6CB. For 5CB, whose results are taken from ref 23, the error bars for the computed enthalpy (*H*) are as large as symbols. The experimental clearing temperatures[6] (308.3 and 302 K for 5CB and 6CB, respectively) are indicated with a vertical dashed line.

Some selected thermodynamic and structural properties are reported as a function of temperature *T* in Figures 3 and 4 for 5−6CB and 7−8CB, respectively, and a comparison with some relevant experimental data[6,55−57] is reported in Table 1. As previously found for 5CB,[23,36] a systematic overestimation of the density can be noted for all homologues. Tentatively, this discrepancy may be traced back either to the *ab initio* calculations or to the fitting procedure used to actually produce the FF. It is worth recalling that our approach is not based on any experimental data to obtain the simulation FF. Work is in progress to improve the whole protocol that leads from the *ab initio* calculations to the FF.

However, we note that the dependence of density on temperature and number of aliphatic carbons is satisfactorily accounted for. As to transition enthalpies, considering that their small values are of the same order as the uncertainties on the computed ones (≃0.7 kJ/mol), the agreement with the experimental values may also be considered satisfactory. By looking

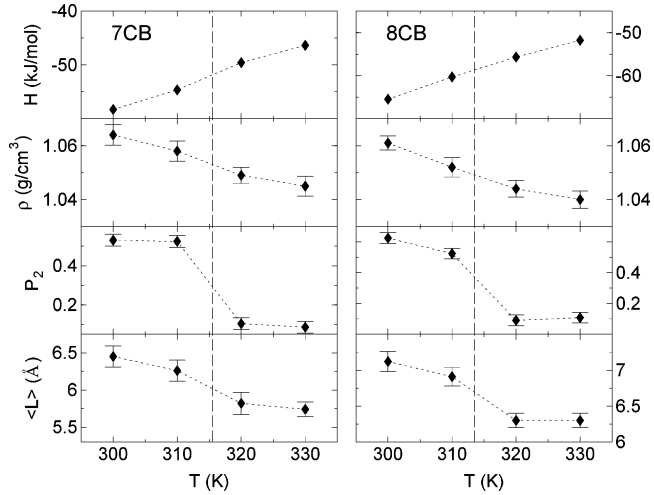

Figure 4. Thermodynamic properties as a function of temperature for 7CB and 8CB. The error bars for the computed enthalpy (*H*) are within the dimensions of the symbols. The experimental clearing temperatures[6] (315.5 and 313.5 K for 7CB and 8CB, respectively) are indicated with a vertical dashed line.

at the first two rows of Figures 3 and 4, one can see that enthalpy or density do not present sharp discontinuities, in agreement with the experimental behavior of weakly first-order transitions, as the nematic to isotropic one. On the contrary, the order and the elongation parameters show a more evident discontinuity in going from the nematic to the isotropic phase. It is worth noting that the experimental transition temperatures are located where the dependence of these properties on *T* is the largest.

The Cb1−Cb1 (see Figure 1) pair correlation function $g(r)$, reported in Figure 5 just below transition temperature ($T^* = T/T_c^{exp} < 1$), is similar in shape to that of ordinary molecular liquids, with a characteristic shell structure. There is a fairly large first band, composed of two peaks, which are better resolved for 5CB and 6CB. A significant difference with respect to ordinary liquids is found for the low number of first neighbors, obtained integrating these curves up to 7 Å: 3 for 5−6CB and about 2.5 for 7−8CB.

The lower panel of Figure 5 reports $G_2(r)$, which shows a strong pair correlation at ≃5 Å and correctly decays to $\langle P_2\rangle^2$ at larger distances. Long-range orientational order can be due to the elongated molecular shape as well as to electrostatic interactions. Indeed, molecules of the *n*CB series carry a fairly large permanent dipole moment (about 5 D in our models), which is mostly due to the electron withdrawing effect of the CN group. Hence, we focused our attention on the N−N pair correlation function g_{NN} and on $G_1(r)$ to observe how much the microscopic structure changes in passing from the isotropic to the nematic phase; in Figure 6, they are reported for 8CB. Because $G_1(r)$ is negative up to 5 Å, molecules in the first coordination shell prefer antiparallel like arrangements. However the G_1 values are well higher than −1, which corresponds to a perfect antiparallel alignment, indicating that significant deviations from this idealized configuration are still present. The pair correlation decreases rapidly with the distance, and finally, the null asymptotic value confirms that there is no spontaneous polarization in the bulk phase. Similar results were found also for all the lower homologues. Because the curves of Figure 6 at 310 K (nematic) and 330 K (isotropic) are rather similar, it appears that the isotropic−nematic transition does not dramatically alter the short-to-medium-range structure.

Figure 7 collects some of our results and some available experimental data concerning the odd−even effect in the *n*CB

TABLE 1: Calculated and Experimental[6,55−57] *n*CB Properties[a]

n	T_c^{calc}	T_c^{exp}	ΔH_c^{calc}	ΔH_c^{exp}	T^*_{calc}	ρ_N^{calc}	ρ_N^{exp}	T^*_{calc}	ρ_I^{calc}	ρ_I^{exp}
5	305	308.3	1.6	0.54	0.973	1.085	1.020	1.038	1.063	0.995
6	300	302.0	−0.3	0.37	0.960	1.076	1.015	1.060	1.056	0.992
7	315	315.5	0.5	0.92	0.983	1.058	0.995	1.045	1.046	0.973
8	315	313.5	0.5	0.84	0.989	1.052	0.983	1.053	1.040	0.963

[a] All temperatures are in K. ΔH_c values, computed at T_c, are in kJ/mol. Calculated densities (g/cm^3) refer to the corresponding T^*_{calc}, and experimental densities are reported at $T^* = 0.985$ and 1.05 in the nematic (ρ_N) and isotropic (ρ_I) phases, respectively.

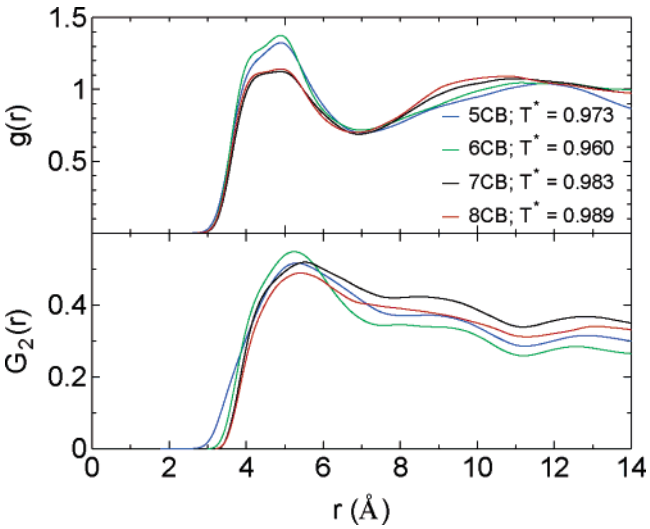

Figure 5. Cb1−Cb1 pair correlation function ($g(r)$, top panel) and orientational pair correlation function ($G_2(r)$, bottom panel) computed for each *n*CB at similar reduced temperatures in the nematic phase.

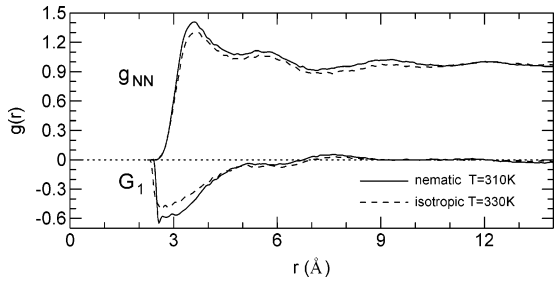

Figure 6. $g_{NN}(r)$ and $G_1(r)$ for 8CB in nematic (solid line) and isotropic (dashed line) phase.

series. The good agreement of the predicted clearing temperatures with the experimental values (top panel) is particularly rewarding in the case of the *n*CB series, where the odd−even effect[5,39,41,42] occurs in a range of temperature (5−10 K) much narrower than in other LC homologue series.[6,22] From the point of view of correctly reproducing the phase diagram of these materials, this accord is certainly encouraging, also because it is confirmed, at least qualitatively, by the behavior of the order parameters $\langle P_2 \rangle$ and $\langle P_4 \rangle$. The odd−even effect was also experimentally found in many other properties of the *n*CB bulk phases, as viscosity in the isotropic phase[40] or rotational diffusion coefficients.[15] Work is in progress to compute the dynamic and transport properties of *n*CBs[54] to test the model capability of providing a correct description of the system dynamics.

The odd−even effect has often[5,31,38,39] found a qualitative explanation by considering only the all-trans (minimum energy) conformations of the side chain, as confirmed also by a detailed study on the interaction energy of the *n*CB dimers.[58] The key

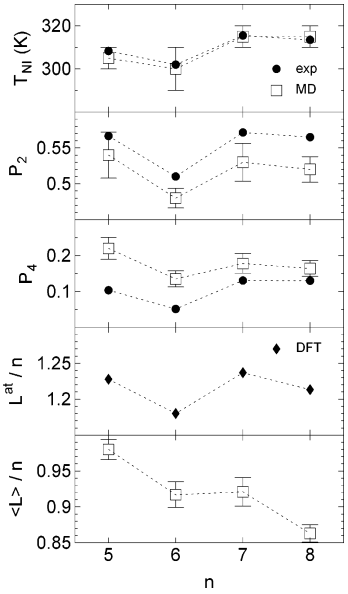

Figure 7. Odd−even effects in the nematic phase of the *n*CB series. Experimental data[6,38] are reported with filled circles and refer to $T^* = 0.985$; empty squares (MD) and filled diamonds (DFT) are used for the computed properties. The latter refer to the reduced temperatures T^*_{calc} reported in Table 1 for the nematic phase.

factor is the angle between the Cp3−Cp2 bond and the molecular long axis, which is ≃0° and >50° for odd or even members, respectively. This is evident in Figure 7, where the elongation parameter L divided by the number of carbon atoms is computed in the all-trans conformation (L^{at}) as resulting from DFT single molecule optimization. However, many conformations other than that all-trans are populated in the bulk phase, so that a more extensive investigation on the conformational behavior is in order.

3.3. Chain Conformations. The softest degrees of freedom in an *n*CB molecule are[23] the dihedral angles between the aromatic core and the chain and the $(n - 2)$ torsional angles of the *n*-carbon aliphatic chain.

From the MD production runs, it turns out that the average value of the formers do not vary appreciably either along the series or across the nematic−isotropic transition, their average values being ≃35° and 90°, respectively. On the contrary, the aliphatic chain dihedrals may assume three different values, namely ±60° (gauche) and 180° (trans). The distribution of these torsions appears to be strongly dependent on the number of aliphatic carbons and on the resulting phase.

Table 2 collects the results of the conformer population of the *n*CB series. Only the all-trans and the conformers with one gauche state are reported as they cover more than half of the total population. The good agreement between the available experimental[37] and MD computed results extends to all the most populated conformations. As already observed for 5CB,[23,36] for all homologues, the chains tend to increase the all-trans

TABLE 2: Populations of Some Conformational States of Nematic (N) and Isotropic (I) Phases of *n*CBs[a]

5CB				
conf	N-MD (%)	I-MD (%)	N-exp (%)	I-exp (%)
ttt	35	26	33	23
gtt	5	6	10	17
tgt	18	17	23	17
ttg	20	22	14	17

6CB			7CB		
conf	N-MD (%)	I-MD (%)	conf	N-MD (%)	I-MD (%)
tttt	23	15	ttttt	17	11
gttt	3	3	gtttt	2	2
tgtt	11	9	tgttt	7	6
ttgt	8	10	ttgtt	4	5
tttg	14	10	tttgt	9	6
			ttttg	8	7

8CB				
conf	N-MD (%)	I-MD (%)	N-exp(%)	I-exp(%)
ttttt	13	9	11	6
gttttt	1	1	2	4
tgtttt	6	5	7	4
ttgttt	3	3	3	4
tttgtt	5	5	6	4
ttttgt	4	4	5	4
tttttg	8	6	7	4

[a] MD data (this work and ref 23) were computed at the reduced temperatures T^*_{calc} reported in Table 1. Experimental data reported for 5CB and 8CB are derived from NMR spectroscopy.[37]

TABLE 3: All-Trans Populations (p_N^{at}, p_I^{at}), Extended All-Trans Populations (p_N^{Σ}, p_I^{Σ}) and Elongation Parameters ($\langle L\rangle_N$, $\langle L\rangle_I$), Computed for the *n*CB Series, in the Nematic (N) and Isotropic (I) Phases[a]

n	p_N^{at} (%)	p_I^{at} (%)	p_N^{Σ} (%)	p_I^{Σ} (%)	$\langle L\rangle_N$ (Å)	$\langle L\rangle_I$ (Å)
5	30.2	23.6	30.2	23.6	4.9	4.7
6	23.0	15.5	36.9	31.1	5.5	5.1
7	16.9	10.6	36.9	30.1	6.5	5.7
8	12.7	8.5	27.9	24.2	6.9	6.3

[a] For each *n*CB, N and I values refer to the reduced temperatures T^*_{calc} reported in Table 1.

population in the nematic phase with respect to the isotropic liquid. Though the shift of the gauche state from the first to the last position (e.g., from gttt to tttg in 6CB) is not accompanied by a monotonic trend in the population, the conformer with the last dihedral in the gauche state is generally favored. This could be expected as it is the less hindered rotation, because it induces the smallest reduction of the chain elongation.

In Table 3, the all-trans percentage p^{at} and the mean elongation parameter $\langle L\rangle$ are reported for each *n*CB in the nematic and in the isotropic phases. The $\langle L\rangle$ values confirm the tendency of these nematogens to assume on average more elongated conformations in going from the isotropic to the orientationally ordered phase. Even if no odd−even effect is apparent for the $\langle L_N\rangle$ values along the series, a typical odd−even alternation results when the elongation parameter is divided by the number of carbons, as shown in the bottom panel of Figure 7.

Turning to the chain dihedral distributions, as the number of possible conformations is 3^{n-2}, it is expected that p^{at} is bound to decrease as *n* increases, so that a sensible comparison through the series needs a sort of normalization. With this aim, we consider the extended percentages p^{Σ}, reported in Table 3, which are obtained by considering all conformations whose R_L lies in the $R_L^{at} \pm 0.8$ range, where R_L^{at} is R_L computed in the all-trans arrangement. The 0.8 value was chosen as it is the difference between R_L^{at} and the ratio R_L computed for the second most populated conformer.

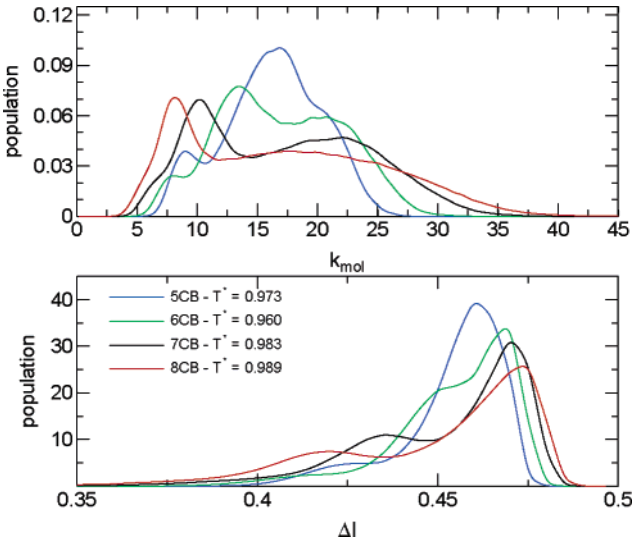

Figure 8. Anisotropy of the inertia tensor of *n*CB in nematic phase: upper panel κ_{mol} (as defined in eq 10), lower panel ΔI (eq 11).

Two major conclusions can now be drawn by looking at Table 3. First, the chains tend to assume more elongated (rodlike) conformations in the nematic phase, through the increase of the trans population and the summed up p_N^{Σ}. Second, despite the all-trans arrangement being less favored on increasing the number of carbons, the extended p^{Σ} is almost constant along the series, confirming that the all-trans low population is just a consequence of the larger number of conformers available.

The distribution of chain conformers determines the molecular shape and also affects the dynamics, through the value of the moments of inertia. Some interesting information can be gained from the behavior of κ_{mol} in the nematic phase along the series (Figure 8). From 5CB to 8CB, single molecule inertia ratios show a neat double peak: the lower one is gradually absorbed in the higher and shifts to smaller values. In higher homologues, there is an increase of the geometric mean of I_1 and I_2, and in fact, the right shoulder of the distribution moves to higher κ values within the series. Somewhat unexpected is the position of the main peak, which shifts to smaller values in higher homologues: this means that on average I_3 increases faster than $\sqrt{I_1 I_2}$. This result can be explained by considering that the molecular tails are not aligned with the long molecular axis: every additional Cp2 group increases the I_3 component of the inertia tensor, thus lowering κ_{mol}. In a condensed phase, the enhanced probability of entanglement when a longer alkyl chain is present combines with this effect, leading to a hindered spinning motion. The κ_{mol} mean value has no clear monotonic behavior; in fact, from 5CB to 8CB it assumes very close values: 16.3, 16.9, 17.4, 17.3.

Analogous conclusions can be drawn from the inertia anisotropy parameter ΔI shown in the lower panel of Figure 8: in the series, curves become progressively broader, and larger values are caused by the enhanced inertia of longer molecules, as also reported in ref 22 for cynnamates. Although most probable values are very similar in cynnamates and *n*CB, we cannot spot any evidence of an odd−even effect. Presumably, this depends on the different molecular structure, as the "heavy"

terminal benzene group, which can be out of plane in cynnamates, is replaced here by a much lighter methyl group. The same reason might explain the reduced size of the odd−even effect of clearing temperatures in *n*CB.

4. Conclusions

The results presented above are a first group from a comprehensive set of MD simulations aimed at investigating static and time dependent properties of condensed phases of *n*CBs. There are two principal motivations behind this study. One is to test the ability of the FRM approach to provide chemical detail descriptions of the interactions between such mesogenic molecules that are accurate enough to make it worth attempting to compare with experimental data. The second is to exploit the wealth of data collected in the MD runs to elucidate the microscopic processes underlying the measured values of macroscopic observables.

With the exception of density, which is overestimated for all thermodynamic states considered of about 6%, the calculated thermodynamic and structural properties, e.g., transition enthalpies and orientational order parameters P_2 and P_4, agree with the corresponding experimental values in a way that supports our confidence in the quality of our model FF. A key property that should be reproduced by simulation is the clearing temperature, as it marks the upper limit of existence of the nematic phase, which has to be appropriate for the desired application. Quantitative structure−property relationship approaches have been pursued to predict transition temperatures for liquid crystalline phases, on the basis of a set of geometric, electronic, and topological descriptors encoding the molecular structure.[59] A 10-descriptor model predicted clearing temperatures of an external set within 5.4 K. Although we did not attempt to outline the phase boundaries of our model systems by free energy calculations, the clearing temperatures obtained by a temperature scan do agree well with the experimental data. As a consequence, also the odd−even effect of these properties is correctly reproduced. This is quite an encouraging achievement, if we consider that clearing temperatures of the *n*CBs alternate in a much narrower range (10 K) than in other homologue series, e.g., the amino-cynnamates, where they can cover a range of about 100 K. For the latter series, the odd−even effect had already successfully been reproduced,[22] so it appears that present day atomistic MD modeling is able to reliably capture rather subtle features of these materials. This is certainly related to the possibility of using adequate numbers of molecules and observing the system for at least some tens of nanoseconds. The latter requirement appears to be the most stringent to gauge the quality of a simulation, as our results, as well as that of Berardi et al.,[22] show that P_2 keeps drifting on a 10 ns time scale during equilibration. In a previous paper,[23] we observed that three samples of 5CB under identical thermodynamic conditions, and rather different initial values of P_2, were able to recover a common P_2 value after 30 ns. Broadly speaking, the time scale of the dynamics is similar for the *n*CB homologues studied here, so we assume that simulations of that length should provide reliable results. The size dependence on the results seems more contradictory, as some authors have observed it[60] and others did not.[61] Of course, size matters, for no long-range fluctuations can be observed in too small a system and the dynamics might also be affected. We are currently investigating[54] the system size effect on models of 8CB consisting of 768 and 1536 molecules, i.e., 4 and 8 times larger than that employed here. This study might give useful information, in particular on the dependence of the smectic phase stability on the number of layers. As already mentioned,[54] the extension of the validation process of the FF to single-molecule and collective dynamic properties is underway and will certainly provide another demanding test of its accuracy. On more general grounds, further developments will include a new approach to the description of the intramolecular part of the force field, a key requirement for an accurate modeling of these materials.

References and Notes

(1) Pelzl, G.; Diele, S.; Weissflog, W. *Adv. Mater.* **1999**, *11*, 707.
(2) Fodor-Csorba, K.; Vajda, A.; Galli, G.; Jákli, A.; Demus, D.; Holly, S.; Gács-Baitz, E. *Macromol. Chem. Phys.* **2002**, *203*, 1556.
(3) Chan, L.; Gray, G.; Lacey, D. *Mol. Cryst. Liq. Cryst.* **1995**, *123*, 185.
(4) Gray, G.; Herrison, K.; Constant, J.; Hulme, D.; Kirton, J.; Raynes, E. *Liquid crystals and ordered fluids*; Johnson, J. F., Porter, R. S., Eds.; Plenum Press: New York, 1974.
(5) Gray, G. W.; Mosley, A. *J. Chem. Soc., Perkin Trans. 2* **1976**, *1*, 97.
(6) Béguin, A.; Billard, J.; Bonamy, F.; Buisine, J.; Cuivalier, P.; Dubois, J.; Barny, P. L. *Mol. Cryst. Liq. Cryst.* **1984**, *115*, 119.
(7) deGennes, P.; Prost, J. *The Physics of Liquid Crystals*, 2nd ed.; Oxford University Press: Oxford, U.K., 1993.
(8) Atomistic simulation and modeling of smectic liquid crystals; In *Advances in the Computer Simulations of Liquid Crystals*; NATO ASI series; Pasini, P., Zannoni, C., Eds.; Kluwer: Dordrecht, Germany, 2000.
(9) Demus, D., Goodby, J., Gray, G. W., Spiess, H. W., Vill, V., Eds. *Handbook of Liquid Crystals*; Wiley-VCH: Weinheim, Germany, 1998; Vol. 1.
(10) Chandrasekhar, S. *Liquid Crystals*; Cambridge University Press: Cambridge, U.K., 1977.
(11) Collings, P.; Hird, M. *Introduction to Liquid Crystals*; Adam Hilger: Bristol, U.K., 1997.
(12) deJeu, W. *Physical Properties of Liquid Crystalline Materials*; Gordon and Breach Science Publishers: New York, 1980.
(13) deJeu, W. *Solid State Phys., Suppl.* **1978**, *14*, 109.
(14) Matsushita, T.; Koseki, S. *J. Phys. Chem. B* **2005**, *109*, 13493.
(15) Siedler, L.; Hyde, A.; Petrick, R.; Leslie, F. *Mol. Cryst. Liq. Cryst.* **1983**, *90*, 255.
(16) *Advances in the Computer Simulations of Liquid Crystals*; NATO ASI series; Pasini, P., Zannoni, C., Eds.; Kluwer: Dordrecht, Germany, 2000.
(17) *Computer Simulations of Liquid Crystals and Polymers*; NATO ASI series; Pasini, P., Zannoni, C., Zumer, S., Eds.; Kluwer: Dordrecht, Germany, 2005.
(18) Wilson, M. *Int. Rev. Phys. Chem.* **2005**, *24*, 421.
(19) Care, C.; Cleaver, D. *Rep. Prog. Phys.* **2005**, *68*, 2665.
(20) Glaser, M. A. Atomistic simulation and modeling of smectic liquid crystals; In *Advances in the Computer Simulations of Liquid Crystals*; NATO ASI series; Pasini, P., Zannoni, C., Eds.; Kluwer: Dordrecht, Germany, 2000.
(21) Lansac, Y.; Glaser, M.; Clark, N. *Phys. Rev. E* **2001**, *64*, 051703.
(22) Berardi, R.; Muccioli, L.; Zannoni, C. *ChemPhysChem.* **2004**, *5*, 104.
(23) Cacelli, I.; Prampolini, G.; Tani, A. *J. Phys. Chem. B* **2005**, *109*, 3531.
(24) Jorgensen, W.; Tirado-Rives, J. *J. Phys. Chem. B* **1988**, *110*, 1657.
(25) Cornell, W.; Cieplak, P.; Bayly, C.; Gould, I.; Merz, K.; Ferguson, D.; Spellmeyer, D.; Fox, T.; Caldwell, J.; Kollmann, P. *J. Am. Chem. Soc.* **1995**, *117*, 5179.
(26) Brooks, B. R.; Bruccoeri, R. E.; Olafson, B. D.; States, D. J.; Swaminanthan, S.; Karplus, M. *J. Comput. Chem.* **1983**, *4*, 187.
(27) Hermans, J.; Berendsen, H.; van Gusteren, W.; Postma, J. *Biopolymers* **1984**, *23*, 1.
(28) Yakovenko, S.; Muravski, A.; Eikelschulte, F.; Geiger, A. *Liq. Cryst.* **1998**, *24*, 657.
(29) Hautpmann, S.; Mosell, T.; Reiling, S.; Brickmann, J. *J. Chem. Phys.* **1996**, *208*, 57.
(30) L. Cheung, D.; Clark, S.; Wilson, M. *Chem. Phys. Lett.* **2002**, *356*, 140.
(31) Capar, M.; Cebe, E. *Phys. Rev. E* **2006**, *73*, 061711.
(32) Cacelli, I.; Cinacchi, G.; Prampolini, G.; Tani, A. Computer Simulation of Mesogen with ab initio Interaction Potentials; In *Novel Approaches to the Structure and Dynamics of Liquids. Experiments, Theories and Simulation*; Samios, J., Durov, V., Eds.; Kluwer: Dordrecht, Germany, 2004.
(33) Amovilli, A.; Cacelli, I.; Cinacchi, G.; De Gaetani, L.; Prampolini, G.; Tani, A. *Theor. Chem. Acc.*, to be published.

(34) Amovilli, C.; Cacelli, I.; Campanile, S.; Prampolini, G. *J. Chem. Phys.* **2002**, *117*, 3003.
(35) Bizzarri, M.; Cacelli, I.; Prampolini, G.; Tani, A. *J. Phys. Chem. A* **2004**, *108*, 10336.
(36) De Gaetani, L.; Prampolini, G.; Tani, A. *J. Phys. Chem. B* **2006**, *110*, 2847.
(37) Emsley, J.; Luckhurst, G.; Stockley, C. *Proc. R. Soc. London, Ser. A* **1982**, *381*, 117.
(38) Kobinata, S.; Kobayashi, T.; Yoshida, H.; Chandani, A.; Maeda, S. *J. Mol. Struct.* **1986**, *146*, 373.
(39) Ojha, D.; Kumar, D.; Pisipati, V. *Cryst. Res. Technol.* **2002**, *37*, 881.
(40) Jadzin, J.; Lech, R. D. T.; Czechowski, G. *J. Chem. Eng. Data* **2001**, *46*, 110.
(41) Karat, P.; Madhusadana, N. *Mol. Cryst. Liq. Cryst.* **1976**, *36*, 51.
(42) Karat, P.; Madhusadana, N. *Mol. Cryst. Liq. Cryst.* **1977**, *90*, 255.
(43) Wiener, S. J.; Kollmann, P. A.; Nguyen, D. T.; Case, D. A. *J. Comput. Chem.* **1986**, *7*, 230.
(44) Paschen, D.; Geiger, A. *MOSCITO 3.9*; Department of Physical Chemistry: University of Dortmund, Germany, 2000.
(45) Berendsen, H. J. C.; Postma, J. P. M.; van Gusteren, W. F.; Di Nola, A.; Haak, J. R. *J. Chem. Phys.* **1984**, *81*, 3684.
(46) Becke, A. *J. Chem. Phys.* **1993**, *98*, 5648.
(47) Ryckaert, J. P.; Ciccotti, G.; Berendsen, H. J. C. *J. Comput. Phys.* **1977**, *55*, 3336.
(48) Allen, M.; Tildesley, D. *Computer Simulation of Liquids*; Clarendon: Oxford, U.K., 1987.
(49) Darden, T.; York, D.; Pedersen, L. *J. Chem. Phys.* **1993**, *98*, 10089.
(50) Essmann, U.; Perera, L.; Berkowitz, M.; Darden, A.; Lee, H.; Pedersen, L. *J. Chem. Phys.* **1995**, *103*, 8577.
(51) Paolini, G. V.; Ciccotti, G.; Ferrario, M. *Mol. Phys.* **1993**, *80*, 297.
(52) *The Molecular Dynamics of Liquid Crystals*; NATO ASI series; Luckhurst, G. R., Veracini, C. A., Eds.; Kluwer: Dordrecht, Germany, 1994.
(53) Bates, M.; Luckhurst, G. *J. Chem. Phys.* **1999**, *110*, 7087.
(54) Cacelli, I.; De Gaetani, L.; Prampolini, G.; Tani, A. Work in progress.
(55) Sandmann, M.; Hamann, F.; Wurflinger, A. *Z. Naturforsch.* **1997**, *52*, 739.
(56) Sandmann, M.; Wurflinger, A. *Z. Naturforsch.* **1998**, *53a*, 233.
(57) Sandmann, M.; Wurflinger, A. *Z. Naturforsch.* **1998**, *53a*, 787.
(58) Cacelli, I.; De Gaetani, L.; Prampolini, G.; Tani, A. *Mol. Cryst. Liq. Cryst.*, to be published.
(59) Johnson, S.; Jurs, P. *Chem. Mater.* **1999**, *11*, 1007.
(60) Cook, M.; Wilson, M. *Mol. Cryst. Liq. Cryst.* **2001**, *181*, 363.
(61) Wang, Z.; Lupo, J.; Patnaik, S.; Pachter, R. *Comput. Theor. Polym. Sci.* **2001**, *11*, 375.